# Performance and stability of semitransparent OPVs for building integration: A benchmarking analysis

D. Chemisana [a, *], A. Moreno [a], M. Polo [b], C. Aranda [b], A. Riverola [a], E. Ortega [b], Chr. Lamnatou [a], A. Domènech [a], G. Blanco [b], A. Cot [b]

[a] Applied Physics Section of the Environmental Science Department, University of Lleida, Jaume II 69, 25001 Lleida, Spain

[b] COMSA CORPORACIÓN, Av. Roma, 25-27, 08029 Barcelona, Spain

*Total number of words: ~ 5950*

## Abstract

Semitransparent (ST) organic photovoltaics (OPVs) are demonstrating great potential for building integration applications, especially in windows. For that purpose, ST-OPVs should achieve adequate transparency and performance stability. In this regard, the present research deals with the experimental performance of three different building-integrated ST-OPV technologies (technology A: developed in the frame of the present study; technologies B and C: commercial modules). More specifically, spectral transmittance and electrical measurements have been conducted in order to determine the characteristics of the modules for building integration and electricity generation purposes. Results regarding the transmittance reveal that technology A outperforms technologies B and C. The stability analysis of the modules verifies that module C is the most stable one with almost no decrease (3.6%) in the power conversion efficiency (PCE). Furthermore, the PCE of technology B is slightly higher than in the case of technology C, which experiences a PCE degradation of about 10-15% over the whole time period. Finally, technology A presents a 20% reduction in PCE at around 500 hours.

*Keywords: Semitransparent organic photovoltaics (OPVs); Building-integrated systems; Spectral transmittance; Electrical measurements; Stability.*

[*] Corresponding author. E-mail address: daniel.chemisana@macs.udl.cat

## List of symbols and abbreviations

| | |
|---|---|
| Ag | Silver |
| AgNW | Silver nanowire |
| AVT | Average visual transmittance [%] |
| BIPV | Building-integrated photovoltaic |
| DAQs | Data acquisition systems |
| $D_\lambda$ | Spectral distribution [-] |
| Dir | Direct irradiance [$W/m^2$] |
| FF | Fill factor [%] |
| Glob | Global irradiance [$W/m^2$] |
| $I_{out}$ | Current of the OPV modules [A] |
| $I_{sc}$ | Short-circuit current [A] |
| ISOS | International Summit on OPV Stability |
| ITO | Indium tin oxide |
| I-V | Intensity-voltage |
| $J_{sc}$ | Short-circuit current density [$A/cm^2$] |
| $MoO_3$ | Molybdenum trioxide |
| MPPT | Maximum power point tracker |
| OPV | Organic photovoltaic |
| PBTZT-stat--BDTT-8 | Polymer donor from Merck |
| $PC_{71}BM$ | [6,6]-phenyl-C71-butyric acid methyl ester |
| PCBM | [6,6]-phenyl-C61-butyric acid methyl ester |
| PCE | Power conversion efficiency [%] |
| PEDOT | Poly(3,4-ethylenedioxythiophene) |
| PET | Polyethylene terephthalate |
| PSS | Poly(styrenesulfonate) |
| PTBT | Poly(4,8-bis[(2-ethylhexyl)oxy]benzo[1,2-b:4,5-b′]dithiophene-2,6-diyl-alt-3-fluoro-2-[(2-ethylhexyl)carbonyl] thieno[3,4-b]thiophene-4,6-diyl) |
| PWM | Pulse Width Modulation |

| | |
|---|---|
| R.H. | Relative humidity |
| ST | Semitransparent |
| T | Module temperature [$^oC$] or thermal cycling |
| $TiO_2$ | Titanium dioxide |
| UV | Ultraviolet |
| V(λ) | Photopic vision efficiency [-] |
| $V_{cell}$ | Potential of the OPV modules [V] |
| $V_{oc}$ | Open-circuit potential [V] |
| $WO_x$ | Tungsten oxide |
| ZnMgO | Zinc magnesium oxide |

**Greek symbols**

| | |
|---|---|
| $\lambda$ | Wavelength [nm] |
| $\tau$ | Transmittance [-] |
| $\tau_V$ | Visible transmittance in agreement with EN 410:2011 [-] |

## 1. Introduction

In conventional photovoltaic installations, where the modules are based on crystalline silicone, the solar cells are responsible for the highest cost, not only from an economic point of view but also from an environmental perspective. Due to the issues mentioned above (economic and environmental), during the last years there is an increasing interest for organic photovoltaic (OPV) systems. OPVs are considered as a cost-effective technology [1] with reduced environmental impact. Resources and processes involved in OPV manufacturing phase and recycling are expected to demand less energy inputs and therefore, OPVs are expected to be more eco-friendly in comparison with other types of photovoltaic systems which include solar cells with high environmental impact [2]. An additional advantage of the OPVs is the fact that they can be fabricated as thin films, lightweight, semitransparent, free form and flexible, widening the possible applications in comparison to conventional silicon-based photovoltaic panels.

With respect to the electrical performance, in the literature remarkable advances by utilizing bulk heterojunction organic devices that combine donor and acceptor substances in the blend have been reported [3]. Also, molecular optimization to tune the optoelectronic properties of photovoltaic materials by chemical modulation is an effective strategy to enhance efficiency. More specifically, the present efficiency record of 13.1% has been obtained for a cell where the small molecule acceptor was synthesized via fluorination [4]. This impressive value of 13.1%, even to be very high in terms of OPV cells, is quite far from the percentages obtained by silicone cells (values above 20%). Although the efficiency trend is quite optimistic, stability and large-scale production issues are not as advanced as the efficiencies [5]. Currently, an important research effort focuses on stability and degradation of OPV cells [6, 7]. Concerning degradation, degradation mechanisms can be influenced by several factors such as oxidation or hydration/hydrolysis that affect the active layer and electrodes, the diffusion of the electrode materials towards the active layer, etc. Usually the combination and interrelation between those factors arises difficulties in understanding the degradation process [8]. However, despite the drawbacks mentioned above, a recent study demonstrates that OPVs with short lifespans of 3 years and efficiencies of around 2% are competitive against conventional photovoltaic technologies and producing electricity at about 0.19 €/kWh [9].

Regarding Building-Integrated Photovoltaic (BIPV) elements, since OPVs can be printed, the size of the module may perfectly match the desired dimensions where the BIPV element should be installed, independently of the shape. Roll-to-roll printing processes are compatible for manufacturing OPV modules, leading to low manufacturing costs. In addition, OPV color range and transparency are easily tunable by simply changing the light-absorbing organic semiconducting small molecule, the polymer type or the thickness [10], additionally to utilizing transparent electrodes. Among OPVs, semitransparent (ST) modules are those bringing the widest variety of possibilities to position them as a perfect candidate for BIPV applications, e.g. in the frame of window-integrated configurations [11]. Figure 1 shows two different semitransparent modules where the grade of transparency and color variability can be appreciated. Figure 1 (a) illustrates a glass laminated red-like color module (Source: [12]) and Figure 1 (b) presents a photograph of a green-like module (Source: [13]).

**a)** **b)**

**Figure 1**. a) Red-like (Source: Yan et al. [12]) and b) Green-like (Source: Lucera et al. [13]) semitransparent modules.

In the literature, several investigations about the development of improved ST organic devices, mainly based on utilizing new acceptors (*i.e.* non-fullerene acceptors), light-trapping architectures to gain extra photons and new transparent top electrodes (*i.e.* transparent conductive oxide, silver nanowire, carbon nanotube, etc.) can be found. Nonetheless, although the stability of nontransparent organic cells has been investigated, very little attention has been paid to ST-OPVs [11]. Most of the stability investigations about OPVs, in general, are performed under controlled laboratory conditions; however, the most relevant and challenging tests are those under outdoor exposure (where the OPVs will eventually be operating) [14].

In order to fill the gap of the lack of stability studies about ST-OPVs and specially to analyze their performance under outdoor conditions, the present study focuses on the experimental outdoor performance monitoring of three types of ST-OPV modules, two commercially available modules and a module developed in the SOLPROCEL European project [15].

## 2. Experimental set-up

In the frame of outdoor stability testing procedures for building integrated OPV modules, there is no regulation to establish the conditions of the experiments. The closest approach is the International Summit on OPV Stability (ISOS) procedure, where several categories of test protocols are defined: dark (D), outdoor (O), simulated light and stress testing (L) and thermal cycling (T). Among them, the ISOS-O, regarding the exigence in the measurements to be conducted, presents three different levels (1: Basic; 2: Intermediate; 3: Advanced). In Table 1, the main characteristics of ISOS-O setup requirements are summed up [16].

**Table 1.** ISOS-O test setup and testing protocol [16]

| | | ISOS-O-1 | ISOS-O-2 | ISOS-O-3 |
|---|---|---|---|---|
| **Test setup** | Light source | Direct sunlight, no shadows | | |
| | Mounting | Static: facing south and tilted at latitude angle. Tracking: 2-axis | | |
| | Load | MPP tracking (preferred) or Open circuit | | MPP tracking or MPP passive (resistor) |
| | Temperature | Ambient | | |
| | Relative humidity (R.H.) | Ambient | | |
| | Characterization light source | Inside, simulated light | Outside under sunlight | Outside regularly and inside at certain periods |

| | | | | |
|---|---|---|---|---|
| **Testing protocol** | Temp. / R.H. | Monitor ambient values | Monitor nominal operating cell temperature (NOCT) and ambient R.H. | |
| | Solar irradiance and irradiation | Monitor irradiance and calculate accumulated irradiation | | |
| | Current (I) - voltage (V) characterization | Measure short-circuit current and open-circuit potential | Measure IV curves | Refer to IEC 60904-1 [17]. Measure IV curves at irradiances close to 1000 W/m$^2$. |
| | Min. measurement intervals | Daily to weekly | 1/15 min - 1/1 h | Outside: 1/15 min - 1/1 h<br>Inside: weekly or monthly |
| | Characterization temp. | Monitor specimen temperature on backside | | |
| | Charact. irriadiance | Monitor irradiance | | |
| | Wind monitoring | Optional | | Monitor wind speed down to 0.25 m/s |
| | Incident-photon-to-electron conversion efficiency | Optional | | Measure |
| | Note data taken in ranges | Optional | Ambient temperature outside of range 20±15 ºC. Irradiance below 400 W/m$^2$ | Ambient temperature outside of range 20±15 ºC. Irradiance below 400 W/m$^2$.<br>Wind speed outside of range 1±0.75 m/s.<br>For 10 min following wind speeds exceeding 4 m/s<br>Wind direction within ±20º east or west. |

Moreover, in the indicated protocol, there are some recommendations for the data reported. For instance, degradation curves of normalized photocurrent and power conversion efficiency (PCE) should be presented from data collected only under irradiances in the range of 800-1000 W/m$^2$ (to avoid non-linear effects) [16].

The items described above state a proper frame for comparisons between different OPV technologies, independently of the location. Nevertheless, in the case of building-integrated devices some of the requirements are not appropriate or hardly achievable (*i.e.* irradiances above 800 W/m$^2$, or module inclination at latitude angle / tracking, etc.). ISOS-O statements are considered as baseline and they are adapted to the present application of OPV for building façade integration.

The ST-OPV modules were monitored at the Applied Energy Research Centre (CREA) of the University of Lleida (in Spain) which is located in Lleida, at latitude 41.36°N and longitude 0.37°E. Experiments were carried out from the end of July to the beginning of December. Figure 2 illustrates the daily average (line), maximum and minimum (dots) ambient temperatures, R.H. and wind speed (at 2 meters height) jointly with the hourly mean irradiance for the monitored period. It can be noted that ambient temperatures show a big variation from the summer to the end of autumn, ranging from around 30ºC to 2ºC (with considerable thermal amplitude). R.H. registers an important increase from values near to 50% to values almost 100% from the end of October on. This is due to the typical foggy periods reported in Lleida around November. On the contrary, wind speed was very low during the whole time period. Global horizontal irradiance experiences logical trend due to the solar declination evolution with a particular affectation during foggy days.

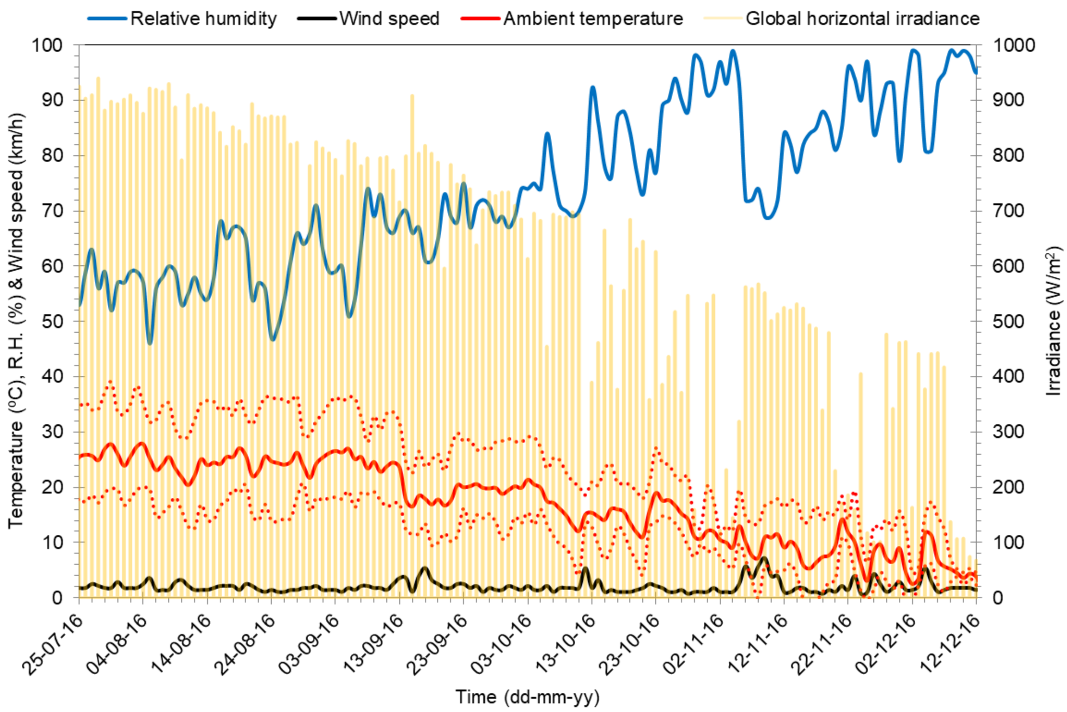


**Figure 2.** Ambient conditions during the monitoring period (location: Lleida, Spain).

The modules were installed facing south at the outdoor testing unit (Fig. 3). It should be noted that the OPVs are enclosed in a double-glass structure in order to better emulate the real building integration and to keep them flat. Spectral and electrical measurements were performed in order to determine the PCE, transparency and stability of such technologies operating under real building-integrated conditions.

The modules were plugged into a specially designed and manufactured maximum power point tracker (MPPT). There are no available commercial MPP trackers for the ranges of currents and potentials of the assessed modules. Electric outputs, at MPP conditions, have been continuously monitored jointly with daily measurements of the intensity-voltage (I-V) curve and spectral-transmittance measurements throughout the experimental campaign. I-V curves were measured outdoors daily once or twice, while for the transmittance measurements the modules were moved to the laboratory, after the sunset, and then they were installed back to the monitoring set-up 5 times during the experimental campaign.

As it can be seen in Fig. 3, a pyranometer (Kipp&Zonen CMP6) has been placed in the middle of the modules in order to register the proper global irradiance received. Furthermore, each module has attached a T-type thermocouple at its rear surface. In addition, in the interior space of the testing unit, the MPPTs jointly with the Data Acquisition Systems DAQs (Campbell Sci. CR3000) and the I-V tracer (Keithley 2460) have been placed.

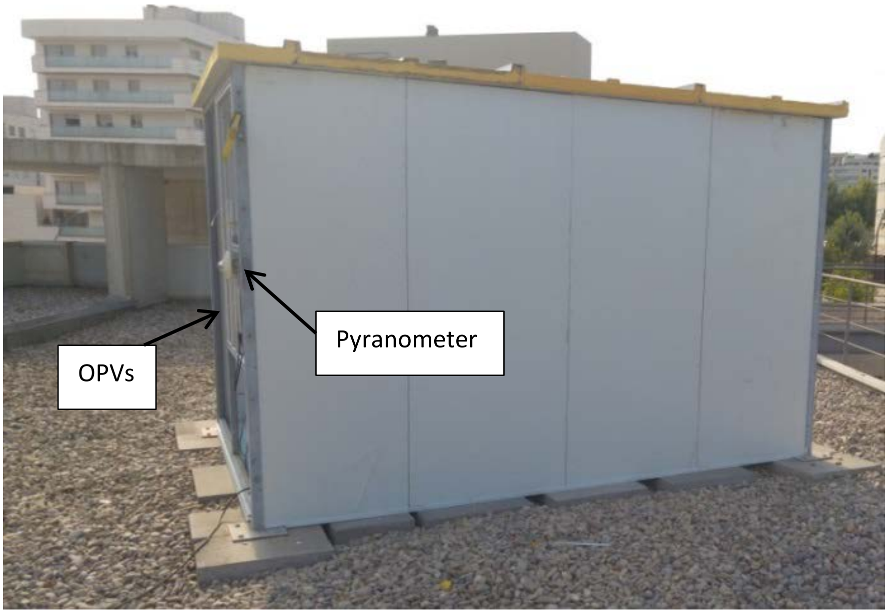


**Figure 3**. The outdoor testing unit (University of Lleida, Lleida, Spain).

The electronics were controlled by an Arduino Mega board, which commands a bipolar junction transistor by utilizing the PWM (Pulse Width Modulation) output based on the PWM value at which the maximum power of the module is delivered. For that purpose, I-V curves were acquired at maximum velocity at different instants from which the maximum power was derived and the PWM frequency was fixed to commute the transistor. In Fig. 4, all the details of the designed circuit are indicated. From Fig. 4 it can be noted that apart of the previously mentioned elements, other important components have also been included (operational amplifier, different filters, diode, etc.). In addition, an important issue is the incorporation of an external battery of 5V in order to ensure signal stability since the 5V output which the board offers presented fluctuations that affected the accuracy of the system. In the same way, the current ($I_{out}$) and the potential ($V_{cell}$) of the OPV modules were monitored with the datalogger for two reasons: 1) because of the simplicity of sampling of all the variables in the same element and 2) due to the fact that Arduino analogical outputs are not sensitive to low values.

Also, the built general circuit allows acquiring data at any time interval and it offers high flexibility, for example, it automatically switches to I-V curve measuring.

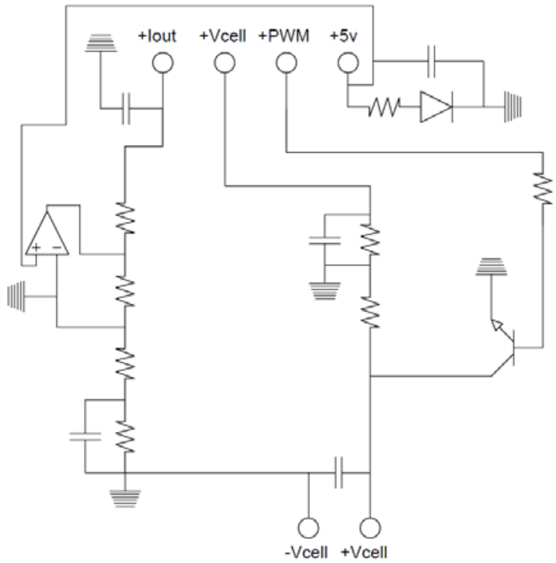


**Figure 4.** Schematic of the maximum power point tracking electronic circuit.

## 3. Characterization of the OPV modules

As it was previously indicated, the characterization of the organic modules consists of two types of tests: 1) the spectral transmission which determines the lighting abilities of the technologies and 2) the evaluation of the electrical performances which leads to reliability and suitability features as generation system. The tests were conducted for three ST-OPV technologies. The modules developed during the project are named as Technology A (2 modules tested: A1, A2), and the commercial ones as Technology B (2 modules tested: B1, B2) and Technology C (1 module tested: C).

Technology A modules have been fabricated with inverted structure and were processed on flexible ITO-Metal-ITO sputtered PET substrates with the layer sequence ZnO nanoparticles / PBTZT-stat-BDTT-8:PCBM / PEDOT:PSS / AgNW. The manufacturing process utilized allows obtaining large area modules with minimum losses with respect to the device at cell level. All the stack layers were processed in ambient conditions via slot-die coating with a heatable head [15]. This represents an important advantage with respect to other manufacturing processes that rely on vacuum and /or present difficulties to print large surfaces.

### 3.1 Spectral transmission

In the field of ST-OPVs, researchers use to refer to the visible region (370-740 nm) based on the Average Visible Transmittance (AVT) parameter [18]. However, for the evaluation of the spectral transmission of the ST-OPVs for building integration applications, it is important to introduce the European Standard EN 410:2011: "Glass in building — Determination of luminous and solar characteristics of glazing" [19]. The standard states how to determine the visible luminous transmittance ($\tau_V$), Eq.(1), considering the relative spectral distribution of illuminant D65 ($D_\lambda$) and the spectral luminous efficiency for photopic vision, $V(\lambda)$ (which ranges from 400 to 700 nm with its peak at 555 nm). The bandwidth defined in the standard comprises the interval where the transmission of the ST-OPV should be enhanced in order to allow a proper vision in the interior spaces.

$$\tau_V = \frac{\sum_{\lambda=380\,nm}^{780\,nm} D_\lambda \tau(\lambda) V(\lambda) \Delta\lambda}{\sum_{\lambda=380\,nm}^{780\,nm} D_\lambda V(\lambda) \Delta\lambda} \tag{1}$$

For the spectral transmission characterization, an Ocean Optics spectrometer has been used, measuring the spectrum transmitted at 5 different points distributed along the module surface (in order to determine the homogeneity of the organic blend). It should be noted that the transmitted light percentage measured does not consider the scattered fraction. Figure 5 illustrates the transmittance spectra measured for the three technologies (A: Fig. 5(a); B: Fig. 5(b); C: Fig. 5(c)) at the five sampling points, indicating that the commercially available modules present slightly less dispersion between the different parts of the module (in comparison to the spectra measured for technology A). In addition, it can be noted that C presents the most uniform behavior, almost overlapping the transmittances for all the sampling points. Moreover, the most important reflected part in all of them was around the blue to green bandwidth; therefore, all the modules appearance is aesthetically similar.

**a)**

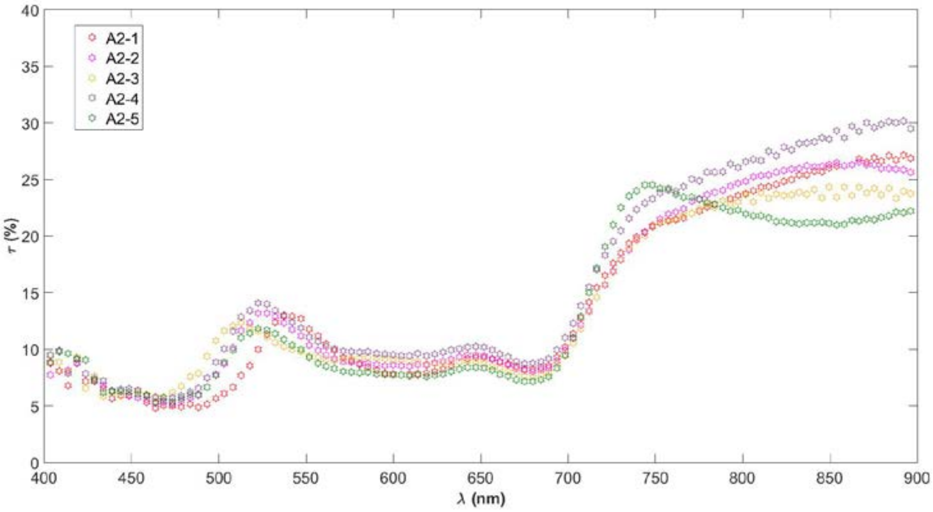


**b)**

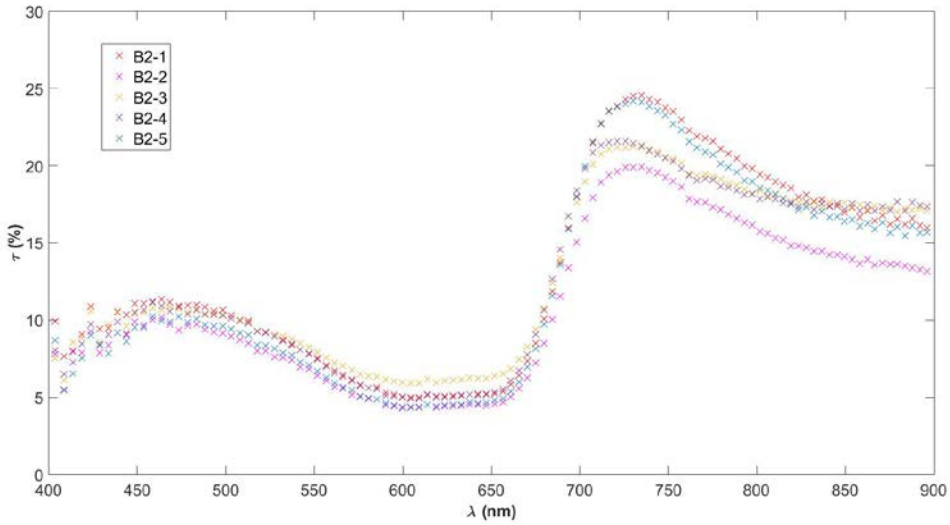


**c)**

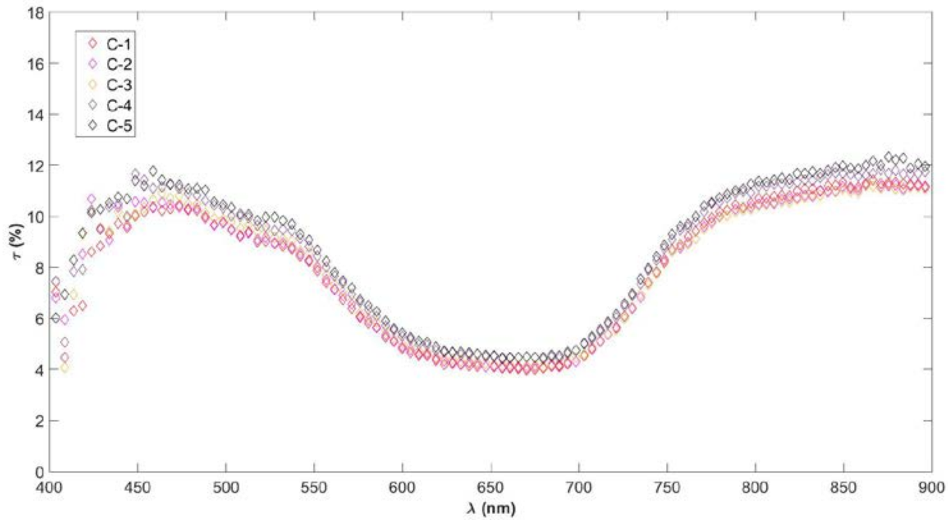


**Figure 5**. The transmittance spectra measured for the three technologies (a: A2; b: B2; c:C) at the five sampling points.

As it was previously highlighted, due to the high flexibility of the photovoltaic elements and in order to better emulate the building-integration conditions, the modules were encapsulated in an extra clear double-glass sandwich to keep them flat and also to perform the function as structural element. In order to more precisely estimate the transmission of the OPV units, the double glass transmission that supports therein each type of technology has been measured. The obtained mean transmittance value for the double glasses was 85.4% for the interval [380-780] nm.

Figure 6 shows the 5-sampling points mean spectral transmittance (corrected with the double-glass transmittance, τ´) for each module technology, measured at the end of the characterization. Also, the curve resulting from the product of the illuminant relative spectral distribution ($D_\lambda$) and the photopic vision efficiency, V(λ), is depicted.

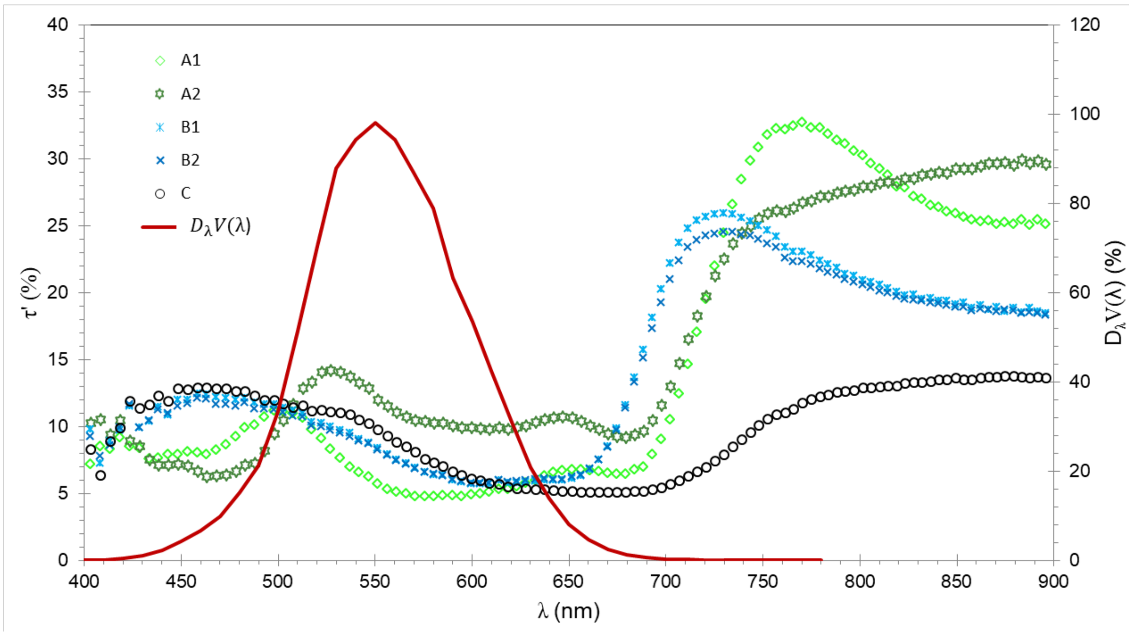


**Figure 6**. Mean spectral transmittances of the modules at the end of the monitoring period and the $D_\lambda V(\lambda)$ curve.

As it can be seen in Fig. 6, the product $D_\lambda V(\lambda)$ is 0 for wavelengths below 400 nm and above 700 nm since $V(\lambda)$ is 0 as well. Consequently, the effective bandwidth where the ST-OPVs should better transmit is limited to the interval [400-700] nm. Under the bandwidth 400-700 nm, the performance of all the technologies is quite stable and lower than that observed from 700 nm on. Conversely, for module C the spectrum presents a quite flat shape for the whole range. Module A2 presents the highest transmittance (11.3%), followed by modules C (9%) and B (8.25% on average). On the other hand, the other module of technology A, A1, registers the lowest transmittance (6.7 %). This fact confirms the previously indicated necessity of improving repeatability in the manufacturing process to obtain more homogenous blends (Table 2).

**Table 2**. Visible luminous transmittance.

| **Tech.** | $\tau_v'$**(%)** |
|---|---|
| A1 | 6.7 |
| A2 | 11.3 |
| B1 | 8.3 |
| B2 | 8.2 |
| C | 9.0 |

In general, for the measured spectra, small changes (regarding the spectral content transmitted) have been observed. Specifically for the photopic range, the shape of the spectral transmission between the initial and final measurements appears to be very similar and the variations seem to be negligible. Table 3 includes the mean transmittances of all the modules A, B and C at the maximum relative luminous efficiency wavelength (555 nm). Concerning the transmittances, these are reported correcting the effect of the double glazing ($\bar{\tau}'$). Also the subscripts *i* and *f* denote the values measured at the beginning and at the end of the experiments, respectively. From the data, it can be pointed out that small variations in spectral transmittance have been registered over the monitoring and technology A (module A2) presents the highest transmittance.

**Table 3**. Spectral transmission values.

| **Tech.** | $\bar{\tau}_i'{}_{555}$ **(%)** | $\bar{\tau}_f'{}_{555}$ **(%)** | \|Difference\| (%) |
|---|---|---|---|
| A1 | 3.8 | 5.3 | 1.5 |
| A2 | 10.6 | 11.5 | 0.9 |
| B1 | 6.3 | 5.5 | 0.8 |
| B2 | 5.9 | 5.3 | 0.6 |
| C | 9.5 | 8.6 | 0.9 |

### 3.2 Electrical performance

#### 3.2.1 Initial electrical characterization

In the present subsection, the electrical characteristic parameters of the modules at the beginning of the monitoring period are analyzed. The modules were placed on a two-axis tracker in order to determine their electrical parameters under stable solar irradiance conditions. Before the monitoring, modules of technologies B and C were stored in dark room environment about three months and modules of technology A were stored one week before the experimental measurements. In the case of the devices developed in the frame of the project (Technology A), two determinations have been included to discern between (1) the behavior after continuous sunlight exposure of ten minutes (in the following notation, this case is indicated as +10 min) and (2) the values measured at the initial time of the exposure (light soaking effects). In Table 4, the measurement conditions, including global irradiance (Glob), direct irradiance (Dir) and module temperature (*T*), along with a summary of the main electrical parameters determined ($J_{sc}$: short-circuit current density, $V_{oc}$: open-circuit potential, *FF*: fill factor and *PCE*: power conversion efficiency) are presented.

**Table 4**. Summary of the main electrical parameters and boundary conditions.

| Technology | *T* (ºC) | Glob (W/m$^2$) | Dir (W/m$^2$) | $J_{sc}$ (mA/cm$^2$) | $V_{oc}$ (V) | *FF* (%) | *PCE*(%) |
|---|---|---|---|---|---|---|---|
| A1 | 23.22 | 810 | 682 | 0.37 | 8.75 | 54.67 | 2.18 |
| A1(+10min) | 24.54 | 834 | 705 | 0.38 | 8.75 | 54.82 | 2.19 |
| A2 | 21.21 | 783 | 672 | 0.34 | 8.84 | 52.92 | 2.03 |
| A2(+10min) | 23.81 | 802 | 675 | 0.35 | 8.90 | 52.99 | 2.06 |
| B1 | 29.08 | 1007 | 875 | 0.99 | 8.12 | 59.19 | 4.72 |
| B2 | 29.11 | 1007 | 874 | 1.00 | 7.59 | 57.57 | 4.34 |
| C | 30.93 | 1012 | 889 | 0.19 | 39.28 | 44.32 | 3.27 |

Technology A has advantageous aspects regarding manufacturing and scalable efficiencies from cell to module level; however, as it can be noticed in Table 4, the PCE values achieved are half of the values of the commercial technology B. The main reason which leads to this lower efficiency is the fact that the organic tandem photogenerates half of the short circuit current density produced by B modules (it should be considered that the outdoor irradiance is 25% higher for technology B; thereby, by assuming a direct proportionality between irradiance and short circuit current, the values for A modules should be close to near 0.45 $mA/cm^2$ with the same irradiance). Nevertheless, the commercial technology C outperforms technology A due to the high potential achieved (since both short-circuit current density and fill factor are lower than for technologies A and B).

### 3.2.2 Stability analysis

Once the modules were initially characterized, they were installed in the façade-like outdoor experimental testing unit (described in section 2) in order to start the continuous daily monitoring for sunny days. During cloudy days, weekends and on holidays (2 weeks in August) the modules were kept under open-circuit conditions. Leaving the OPVs at open-circuit conditions is a circumstance that a building integrated system may often experience (either the regulator opens the circuit in a configuration with batteries or the inverter opens the circuit in a direct consumption scheme when there are no loads). In addition, the ISOS-O protocol considers open-circuit conditions for its levels 1 and 2 (Table 1). Fig. 7 plots the global irradiance evolution throughout the monitoring and it can be noticed the increase in the irradiance due to the seasonal-lower-solar-altitude effect approaching the winter solstice. On the other hand, it can be pointed out that the ISOS recommended selection of data in the interval [800-1000] $W/m^2$ for the degradation curves of normalized photocurrent and PCE [16] is hardly achievable for building façade integrated systems (only data from the end of October onwards are above 800 W/m$^2$).

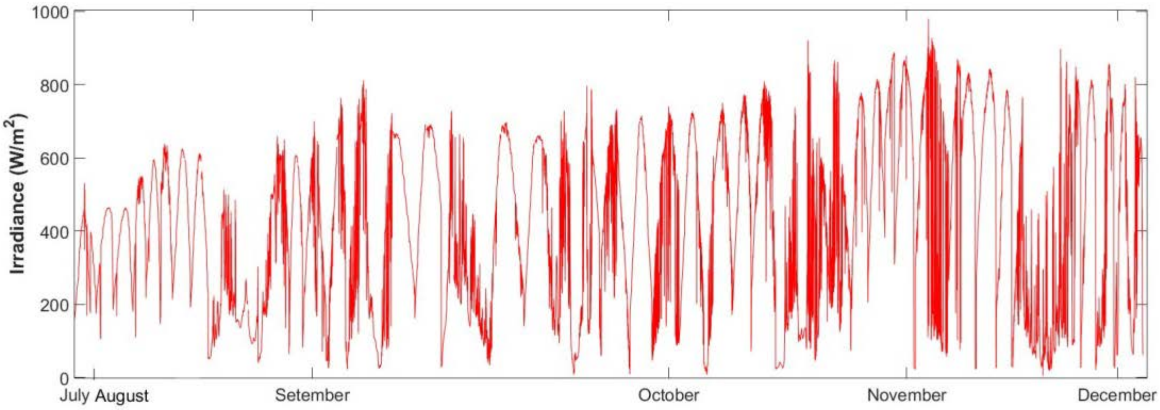


**Figure 7**. Global irradiance profile at the plane of the modules.

In the following graphs, some representative results which illustrate how the modules perform are presented.

The first result reported is the short circuit current sensitivity against solar irradiance. This indicates the photogeneration proportionality with the solar radiation which should reflect a linear tendency. All the modules presented the expected performance, exhibiting a very good fit with correlation coefficients above 0.9. Figure 8 illustrates the average short circuit currents for each type of technology.

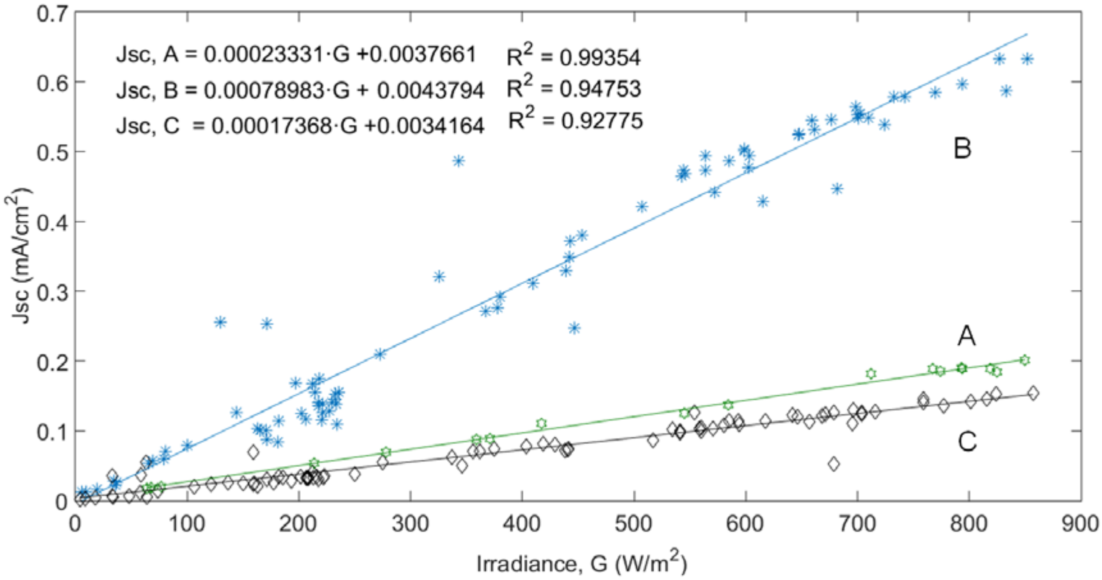


**Figure 8**. The average short circuit currents for each type of technology (A, B and C) vs. irradiance.

The correlation equations (Fig. 8) show the mean short circuit current density of the modules for an irradiance range registered during the monitoring period (slope) which is representative of the average spectral response that should be expected for a real ST-OPV for building integration applications. The slope value has to be corrected by a factor of $10^4$ to homogenize the surface units between irradiance and short-circuit current. Therefore, the modules A and C present average spectral response values of 2.33 $mA\cdot W^{-1}$ and 1.74 $mA\cdot W^{-1}$ (respectively) whilst B modules achieve a mean value more than three times higher than those of modules A and C (7.90 $mA\cdot W^{-1}$).

On the other hand, in Fig. 9 the maximum power output for the modules A is illustrated. Fig. 9(a) refers to the module A1 and Fig. 9(b) refers to the module A2. From Fig. 9 it can be seen that both modules present similar tendency, decreasing the power output quite sharply at the first half of the monitoring and stabilizing the reduction at the second half. This remark is supported by the efficiency evolution which is depicted in Fig. 10.

a) b)

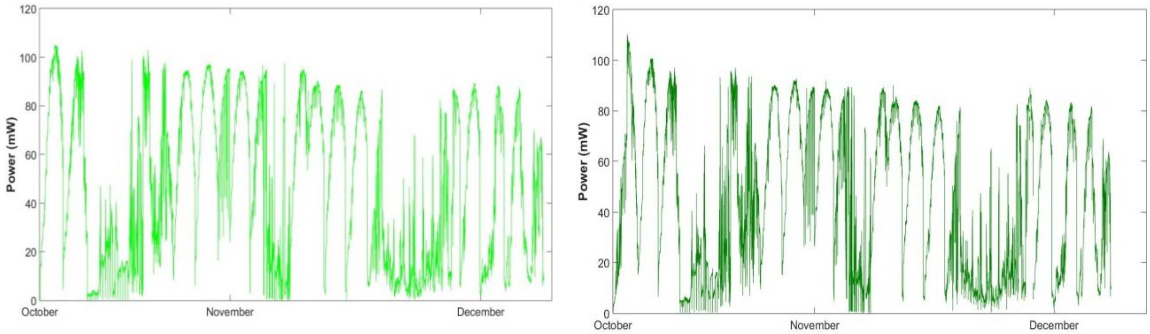


**Figure 9**. The maximum power output for modules A1 (a) and A2 (b).

Fig. 10(a) demonstrates the efficiency evolution observed for module A2 (for module A1 analogous results were obtained). The efficiency values plotted, measured with the I-V tracer, were previously filtered eliminating all with irradiance values lower than 450 W/m$^2$ in order to facilitate comprehension and due to the fact that those points registered more noise. A quadratic polynomial fitting is applied denoting that, as it has been indicated above, the efficiency reduction considerably decelerates for the second half of the monitoring. It should be noted that this effect was expected by the SOLPROCEL-project partners.

For technology B, the efficiency reduction over the time period is more linear than in the case of A modules. In Fig. 10(b), the efficiency evolution of module B1 is illustrated. The points included, as in the case of Fig. 10(a), were measured by means of the I-V tracer and a post-processing was applied for selecting values with incident irradiances equal or higher than 450 W/m$^2$.

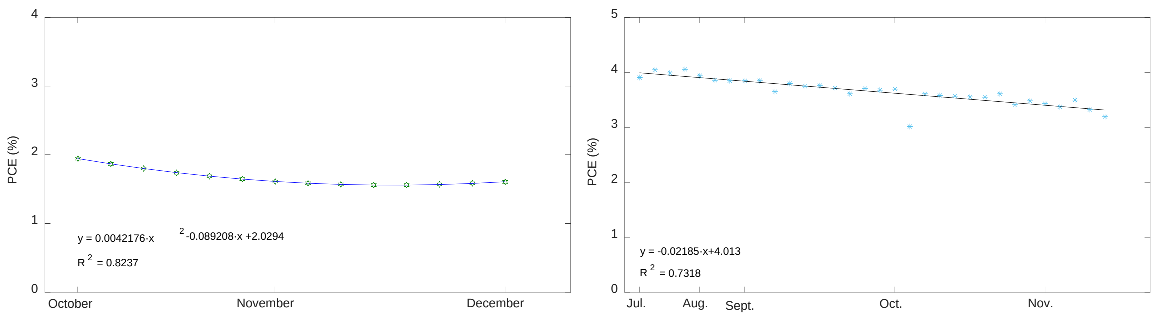


a) b)

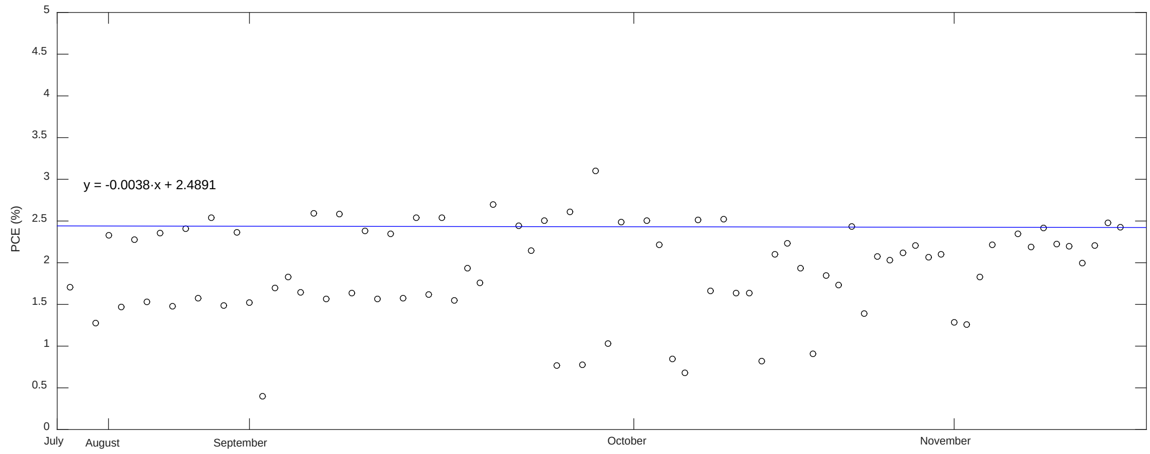


c)

**Figure 10**. The efficiency evolution for modules A2 (a),B1 (b) and C (c).

Finally, Fig. 10 (c) shows the efficiency evolution for module C, but in this case all the measurements conducted with the I-V tracer are included and the fitting is applied only to those obtained with irradiances equal or higher than 450 W/m$^2$. It should be noted that technology C is the one achieving the lower efficiency reduction with an almost flat tendency. The correlation coefficient is not included in order to avoid confusion since the cloud of points is wider and the fitting is conducted regarding to the above mentioned irradiance restriction.

In Table 5, the electrical efficiencies at the beginning (indicated with *i*) and at the end (indicated with *f*) of the experimental campaign are summarized. From Table 5, it can be seen that the highest efficiency reduction is presented by technology A, although this reduction shows a much lower rate of reduction at the second half of the monitoring. In addition, the calculated differences are not far from those reported for modules of technology B. Module C is the one achieving the lowest efficiency reduction.

**Table 5**. Summary of the electrical efficiencies.

| | A1 | A2 | B1 | B2 | C |
|---|---|---|---|---|---|
| ***$PCE_i$* (%)** | 2.083 | 1.944 | 3.991 | 3.722 | 2.569 |
| ***$PCE_f$* (%)** | 1.712 | 1.607 | 3.396 | 3.289 | 2.477 |
| Relative difference (%) | -17.81 | -17.33 | -14.90 | -11.63 | -3.581 |

In the next paragraphs, the I-V curve measurements are expressed normalized in order to compare the differential dynamics of the three technologies on a common basis. For this purpose, the results of the short-circuit current and maximum power have been linearly adjusted to the standard irradiance level of 1000 W/m$^2$. The parameters have been normalized with respect to the initial values measured. Irradiance values range from 520 W/m$^2$ to 825 W/m$^2$ and temperatures are in the interval [25-55] ºC. The hottest temperatures correspond to the summer period and the coldest ones to the end of November-beginning of December.

Figure 11 demonstrates the stability curves of $V_{oc}$ , $J_{sc}$ , *FF* and *PCE.* In the case of the open-circuit potential, it remains quite stable for the technologies A and C. However, for modules B the potential increases slightly. This performance is attributed to the fact that technology B is more sensitive to the temperature than modules A and C. In this way, since the temperature decreases during the experiment the open-circuit potential gradually increases. FF values in all the modules present the same similar dynamic, showing almost no change during the monitoring. On the contrary, short-circuit current and PCE behave similarly, showing three different decay tendencies. The first one regards to the module C, which even presenting more variability in the point cloud, is the most stable (as it is indicated in Table 5) with almost no decrease in the PCE. The second one corresponds to technology B, which decreases slightly more than technology C. Concerning the PCE, a degradation of about 10-15 % is observed over the whole period. Finally, the third one is associated to technology A, which at around 500 hours decays 20% of the PCE. Nonetheless, it seems that A modules experience a certain recovery afterwards, finishing the experiment with a PCE decrease of about 18%.

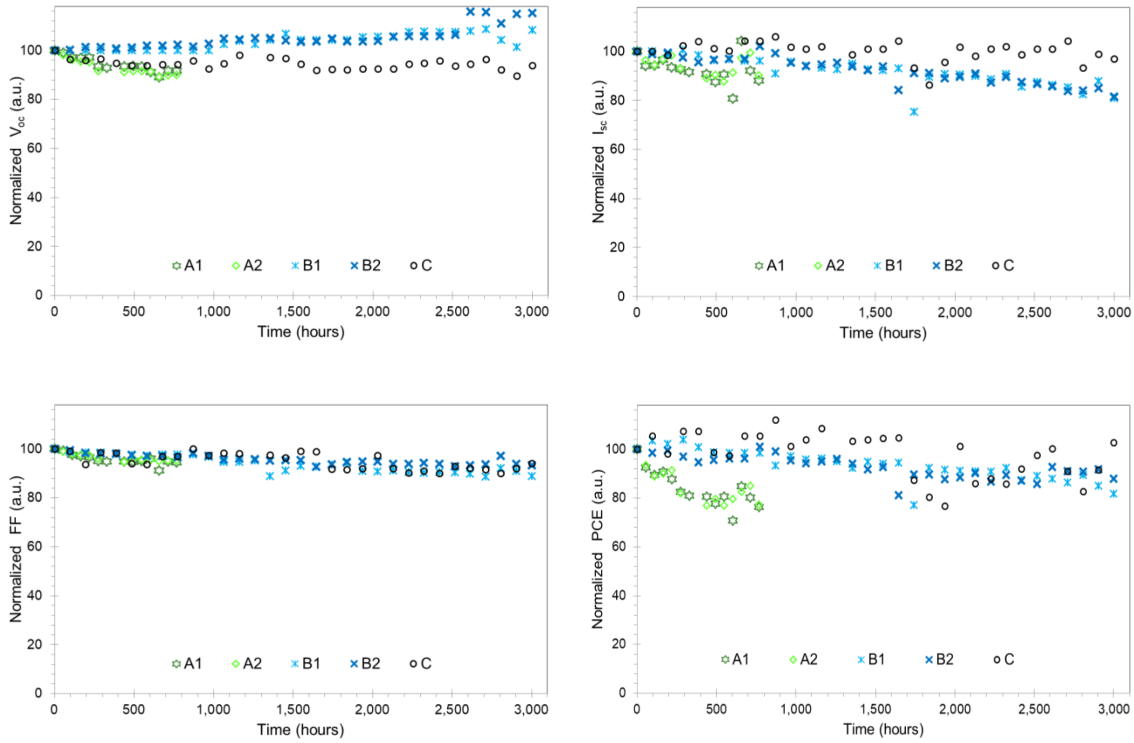


**Figure 11.** Stability curves of short-circuit current, open-circuit potential, fill factor and power conversion efficiency of the 5 OPV modules that have been studied. The parameters are normalized to the initial values registered.

## 4. Comparison with other OPV stability studies

The comparison between ST-OPVs modules is an important aspect to frame and identify the state-of -the-art evolution of a promising but highly changeable technology. This comparison becomes even more essential when one of the main applications of such technology is for building integration. In that case, the customers and installers need to know contrasted results in order to gain confidence in this type of devices. In this regard, it should be highlighted again the necessity of conducting more studies under real outdoor operating condition to demonstrate how ST-OPVs perform.

### 4.1 Light transmission

In the frame of light transmittance, to the authors' knowledge there is no study analyzing the outdoors stability of ST-OPVs in terms of optical parameters. In addition, the ISOS protocol does not refer to this type of characterization [16]. In spite of this fact, some references concerning the transparency tendency of OPVs have been cited. It is indicated that AVT values equal or higher than 25% should be achieved for ST-OPVs applications in windows [20]. In this line, representative results report quite high AVT values (> 50%) and acceptable PCEs over 2% [21-23]. However, efficiency and transmittance performances are confronted since the higher the transmittance the lower the PCE. As a compromise between both parameters a combination of 31% AVT and 10.2% PCE has been recently presented by Jia et al. (2018) [18]. It should be noted that the values reported in the literature are at laboratory scale and at cell level (module PCEs and AVT could be expected to be lower). This makes particularly difficult the comparison with the present study. Also, the results described in section 3.1 refer to the direct transmittance, but in the values found in the literature is difficult to discern if direct or hemispherical transmittances are indicated, and the differences between them may be significant. Moreover, even if the most generalized AVT interval is [370-740] nm depending on the study, the AVT bandwidth is differently defined, for instance in reference [24] the range considered is from 380 nm to 780 nm whilst in study [25] the range includes wavelengths from 400 nm to 700 nm. Based on this argument, it can be seen the necessity of following uniform criteria for the definition of the transparency, for instance the aforementioned EN 410:2011 [19] could be adopted.

### 4.2 Electrical performance

As it has been indicated in the introduction, in the literature very few studies about the stability of ST-OPVs [11] can be found, and there are no investigations regarding outdoor test conditions. A stability laboratory study following the ISOS-L-1 protocol [16] was conducted for a ST-OPV cell utilizing a transparent electrode made of two different transparent PEDOT:PSS Clevios® PH1000 and a combination of PH1000 with $WO_x$. The 8-hours stability tests revealed that the device without $WO_x$ exhibited almost 77.91% degradation of PCE while the device with the introduction of $WO_x$ only suffered a decay of 46.94% from the initial PCE [26]. Romero et al. [27] studied the stability, according to ISOS-L-3 [16], of five different bulk heterojunction configurations made of the copolymer based on PTB7 donor blended with $PC_{71}BM$ acceptor. They pointed out that such types of ST-OPVs (when properly isolated from external agents) show potential to become stable devices. Among ST cells, inverted architectures with isolation and 5-layer deposition demonstrated close to 8 times the lifetime of the same inverted cells without the isolation stack and 400 times longer lifetime than standard ST-OPVs. The time at which the efficiency is 80% of the initial value was found to be at 250 hours for the inverted ST-OPV cell and 1900 hours for the optimum one (inverted with multilayer isolation) [27]. Voroshazi *et al*. [28] conducted light stability tests of ITO-free ST-OPV devices. The transparent electrodes tested, based on $MoO_3$/Ag/$TiO_2$, excluding UV light, degraded similarly to a cell with ITO electrode, demonstrating the feasibility of the proposed transparent electrode. The tests were developed in agreement with ISOS-L-2 protocol, and the devices lost 20% of their initial PCE in less than 50 hours. Finally, Yin et al. [29], studied the stability, according to ISOS-D-1 protocol, of a ST-OPV cell using a ZnMgO-modified cathode combined with a thin $MoO_3$/Ag anode. After 2 months of storage, ST-OPVs demonstrated long lifetime stability retaining over 90% of the initial PCE. Also, good stability was observed after 2 years of storage, maintaining a PCE value of 7.02% and stablishing the high efficiency record for long lifetime ST-OPVs.

It can be appreciated that the described studies regard ST-OPV cells and not modules and, in all the cases, the ISOS protocol is followed either at the laboratory under simulated sunlight or under dark storage. From the results indicated, a wide variation between decay time-periods, ranging from few hours to two years, is observed depending on the experiments that were carried out. In addition, all the cited references present potentiality from several points of view: low-cost transparent electrodes, better isolation structures, etc. The investigations presented are promising, however, they are not mature enough and need more reliability in order to be available on the market.

In the present study, the values obtained are difficult to be compared with those mentioned above since degradations obtained are lower, in general, but the frame is different since in the present work outdoor characterization has been performed.

## 5. Conclusions

In the present study, a comparison between three different ST-OPV technologies (the technology developed in the frame of the SOLPROCEL project and two commercial ones) in order to analyze and compare their efficiency, transparency and stability in an outdoor building-façade environment, has been conducted.

Regarding visible transmittance, a lack of homogeneity in the presentation of results, with the different bandwidths utilized, has been detected. Since one of the potential applications of ST-OPVs is building integration, the adoption of a common protocol for determining transmittances following the European Standard EN 410:2011: "Glass in building- Determination of luminous and solar characteristics of glazing" is suggested.

Measured transmittances over the experimental campaign, for all the photovoltaic modules that have been studied, presented small variations of less than 2% (at 555 nm) between the beginning and the end of the experiments. Technology A showed higher transmittances than the commercial technologies B and C. More specifically, the module A2 presented the highest transmittance (11.3%), followed by modules C (9%) and B (8.25% on average). On the other hand, the other module of technology A (module A1) showed the lowest transmittance (6.7 %).

Concerning the determination of the uniformity of the transmittance along module surface, 5 different points (distributed along module surface) have been measured. The results indicated that the commercially available modules present slightly less dispersion between the different parts of the module than spectra measured for technology A. Between technologies B and C, it can be noted that technology C presents the most uniform behavior (almost overlapping transmittances for all the sampling points).

An important gap regarding stability studies for ST-OPVs, especially in terms of analyzing their performance under outdoor conditions, has been identified. This may be attributed to the fact that this technology is still emerging and it is difficult to scale it up to module level adequate for realistic pre-market studies. In the frame of outdoor stability testing procedures for building integrated OPV modules, there is no regulation to establish the conditions of the experiments. The closest approach is the International Summit on OPV Stability (ISOS) procedure, with its outdoor protocol. Nevertheless, this should be adapted to the specific conditions of building integrated photovoltaics since some requirements and recommendations do not match well for this specific application: inclination of the module, irradiances achieved, etc.

Form the initial electrical characterization, it can be observed that the PCE values obtained by technology A are half of the values achieved by the commercial technology B. The main factor which leads to this lower PCE is the fact that the organic blend generates less than half of the short-circuit current density of the B modules. The commercial technology C outperforms technology A because of the high potential achieved since both the short-circuit current density and the fill factor are lower than for technologies A and B. More specifically, during the monitored period, the mean spectral responses achieved for technologies A and C are 2.33 $mA{\cdot}W^{-1}$ and 1.74 $mA{\cdot}W^{-1}$ respectively whilst B modules achieve a mean value more than three times higher.

With respect to stability, module C is the most stable one with almost no decrease in the PCE (3.6%).  PCE of technology B decays slightly more than for technology C, experiencing a PCE degradation of about 10-15 % over the whole period. Finally, technology A presents a reduction of 20% in PCE in 500 hours. Nonetheless, it seems that A modules experience certain recovery afterwards, finishing the experiment with a PCE decrease of about 18%.

A comparison between the present findings and  other ST-OPVs studies indicates: 1) on the one hand, the necessity of homogenizing results to ease comparisons and 2) on the other hand, a big variability between stability results is denoted, with some modules important PCE decays in few hours and others performing well after 2 year period.

**Acknowledgments:** The authors would like to acknowledge financial support from European Commission 7$^{th}$ Framework Programme (FP7-NMP-2013-SMALL-7).

## 7. References

[1] J. Yu, Y. Zheng, J. Huang, Towards high performance organic photovoltaic cells: A review of recent development in organic photovoltaics, Polymers 6(9) (2014) 2473–2509.

[2] Hengevoss, D., Baumgartner, C., Nisato, G. & Hugi, C. 2016, "Life Cycle Assessment and eco-efficiency of prospective, flexible, tandem organic photovoltaic module", Solar Energy, vol. 137, pp. 317-327.

[3] N. Bristow, J. Kettle, Outdoor performance of organic photovoltaics: Diurnal analysis, dependence on temperature, irradiance, and degradation, J. Renew. Sustain. Energy 7(1) (2015) .

[4] Zhao, W., Li, S., Yao, H., Zhang, S., Zhang, Y., Yang, B. & Hou, J. 2017, "Molecular Optimization Enables over 13% Efficiency in Organic Solar Cells", Journal of the American Chemical Society, vol. 139, no. 21, pp. 7148-7151.

[5] Y. Wang, W. Wei, X. Liu, Y. Gu, Research progress on polymer heterojunction solar cells, Solar Energy Mat. Solar Cell. 98 (2012) 129-145.

[6] Z. Ding, J. Kettle, M. Horie, S.W. Chang, G.C. Smith, A.I. Shames, et al. Efficient solar cells are more stable: The impact of polymer molecular weight on performance of organic photovoltaics, J. Mater. Chem. A 4 (2016)7274-7280.

[7] R. Hansson, C. Lindqvist, L.K.E. Ericsson, A. Opitz, E. Wang, E. Moons, Photo-degradation in air of the active layer components in a thiophene-quinoxaline copolymer: fullerene solar cell, Phys. Chem. Chem. Phys. 18 (2016) 11132-11138.

[8] N. Grossiord, J.M. Kroon, R. Andriessen, P.W.M. Blom, Degradation mechanisms in organic photovoltaic devices, Org. Electronics 13(3) (2012) 432-456.

[9] Mulligan C.J., Wilson M., Bryant G.,Vaughan B., Zhou X., Belcher W.J., Dastoor P.C., A projection of commercial-scale organic photovoltaic module costs, Solar Energy Mater. Solar Cell. 120 (Part A) (2014) 9-17.

[10] B.v. der Wiel, H.J. Egelhaaf, H. Issa, M. Roos, N. Henze, Market readiness of organic photovoltaics for building integration, Materials Research Society Symposium Proceedings. Volume 1639, 2014 2013 MRS Fall Meeting; Boston, MA; United States; 1 December 2013 through 6 December 2013.

[11] Tai, Q. & Yan, F. 2017, "Emerging Semitransparent Solar Cells: Materials and Device Design", Advanced Materials, vol. 29, no. 34.

[12] F. Yan, J. Noble, J. Peltola, S. Wicks, S. Balasubramanian, Semitransparent OPV modules pass environmental chamber test requirements, Solar Energy Mater. Solar Cell. 114 (2013) 214-218.

[13] L. Lucera, F. Machui, H.D. Schmidt, T. Ahmad, P. Kubis, S. Strohm, et al., Printed semi-transparent large area organic photovoltaic modules with power conversion efficiencies of close to 5 %, Organ. Electronics 45 (2017) 209-214.

[14] Gevorgyan, S.A., Madsen, M.V., Dam, H.F., Jørgensen, M., Fell, C.J., Anderson, K.F., Duck, B.C., et al. 2013, "Interlaboratory outdoor stability studies of flexible roll-to-roll coated organic photovoltaic modules: Stability over 10,000 h", Solar Energy Materials and Solar Cells, vol. 116, pp. 187-196.

[15] Solprocel (2016),www.solprocel.eu

[16] Reese, M.O., Gevorgyan, S.A., Jørgensen, M., Bundgaard, E., Kurtz, S.R., Ginley, et al. 2011, "Consensus stability testing protocols for organic photovoltaic materials and devices", Solar Energy Materials and Solar Cells, vol. 95, no. 5, pp. 1253-1267.

[17] IEC 60904, Photovoltaic devices – Part 1: Measurement of photovoltaic current-voltage characteristics. Ed. 2006.

[18] Jia, B., Dai, S., Ke, Z., Yan, C., Ma, W. & Zhan, X. 2018, "Breaking 10% Efficiency in Semitransparent Solar Cells with Fused-Undecacyclic Electron Acceptor", Chemistry of Materials, vol. 30, no. 1, pp. 239-245.

[19] European Standards EN 410:2011, “Glass in building — Determination of luminous and solar characteristics of glazing”, Ed. 2011.

[20] Chen K-S, Salinas J-F, Yip H-L, et al. Semi-transparent polymer solar cells with 6% PCE, 25% average visible transmittance and a color rendering index close to 100 for power generating window applications. Energy Environ Sci. 2012;5:9551–9557.

[21] Chen C-C, Dou L, Zhu R, et al. Visibly transparent polymer solar cells produced by solution processing. ACS Nano. 2012;6:7185–7190.

[22] Chen C-C, Dou L, Gao J, et al. High-performance semi-transparent polymer solar cells possessing tandem structures. Energy Environ Sci. 2013;6:2714–2720.

[23] Xiao X, Lee K, Forrest SR. Inverted, semitransparent small molecule photovoltaic cells. Appl Phys Lett. 2015;107:033901.

[24] Yu, W., Jia, X., Long, Y., Shen, L., Liu, Y., Guo, W. & Ruan, S. 2015, "Highly efficient semitransparent polymer solar cells with color rendering index approaching 100 using one-dimensional photonic crystal", ACS Applied Materials and Interfaces, vol. 7, no. 18, pp. 9920-9928.

[25] Huan, F., Yip, H-L, Cao, Y. 2015, " Polymer Photovoltaics: Materials, Physics, and Device Engineering", Polymer Chemistry Series, The Royal Society of Chemistry.

[26] Kim, H.P., Lee, H.J., Mohd Yusoff, A.R.B. & Jang, J. 2013, "Semi-transparent organic inverted photovoltaic cells with solution processed top electrode", Solar Energy Materials and Solar Cells, vol. 108, pp. 38-43.

[27] Romero-Gomez, P., Betancur, R., Martinez-Otero, A., Elias, X., Mariano, M., Romero, B., Arredondo, B., Vergaz, R. & Martorell, J. 2015, "Enhanced stability in semi-transparent PTB7/PC71BM photovoltaic cells", Solar Energy Materials and Solar Cells, vol. 137, pp. 44-49.

[28] Voroshazi, E., Yaala, M.B., Uytterhoeven, G., Tait, J.G., Andriessen, R.H.A.J.M., Galagan, Y. & Cheyns, D. 2015, "Light stability of ITO-free semi-transparent and

opaque organic photovoltaic devices", 2015 IEEE 42nd Photovoltaic Specialist Conference, PVSC 2015.

[29] Yin, Z., Wei, J., Chen, S.-., Cai, D., Ma, Y., Wang, M. & Zheng, Q. 2017, "Long lifetime stable and efficient semitransparent organic solar cells using a ZnMgO-modified cathode combined with a thin MoO3/Ag anode", Journal of Materials Chemistry A, vol. 5, no. 8, pp. 3888-3899.